Mon. Not. R. Astron. Soc. **000**, 000–000 (0000) Printed 1 February 2008 (MN LATEX style file v1.4)

The SuperCOSMOS Sky Survey. Paper I: Introduction and Description

N.C. Hambly[1], H.T. MacGillivray[1], M.A. Read[1], S.B. Tritton[1], E.B. Thomson[1], B.D. Kelly[2], D.H. Morgan[3] R.E. Smith[3], S.P. Driver[4], J. Williamson[1], Q.A. Parker[1], M.R.S. Hawkins[1], P.M. Williams[1], A. Lawrence[3]

[1] *Wide Field Astronomy Unit, Institute for Astronomy, University of Edinburgh, Blackford Hill, Edinburgh, EH9 3HJ*
[2] *UK ATC, Royal Observatory, Blackford Hill, Edinburgh, EH9 3HJ*
[3] *Institute for Astronomy, University of Edinburgh, Blackford Hill, Edinburgh, EH9 3HJ*
[4] *School of Physics and Astronomy, University of St. Andrews, North Haugh, St. Andrews, Fife, KY16 9SS*

Accepted —. Received —; in original form —

ABSTRACT

In this, the first in a series of three papers concerning the SuperCOSMOS Sky Survey (SSS), we give an introduction and user guide to the survey programme. We briefly describe other wide–field surveys and compare with our own. We give examples of the data, and make a comparison of the accuracies of the various image parameters available with those from the other surveys providing similar data; we show that the SSS database and interface offer advantages over these surveys. Some science applications of the data are also described and some limitations discussed. The series of three papers constitutes a comprehensive description and user guide for the SSS.

Key words: astronomical databases: miscellaneous – catalogues – surveys – stars: general – galaxies: general – cosmology: observations

1 INTRODUCTION

This is the first paper in a series of three concerning the SuperCOSMOS Sky Survey (hereafter SSS) programme[⋆]. This ambitious project aims to digitise the sky in three colours (BRI), one colour (R) at two epochs, via automatic scans of sky atlas photographs. The source photographic material comes from Schmidt telescopes, observations being taken during the second half of the twentieth century (see later). Ultimately we aim to digitise the entire sky, but due to the time required to do so data are being 'released' to the community as they become available. The first release of data consisted of 5000 square degrees of the southern sky at high Galactic latitude ($|b| > 60°$). This became known as the South Galactic Cap (hereafter SGC) survey. All three papers in this series make reference to data from the SGC survey, but are generally relevant to the SSS as a whole. This paper (Paper I) is intended as a general introduction and user guide to the SSS. Paper II (Hambly, Irwin & MacGillivray 2001a) describes image detection, parameterisation, classification and photometry while Paper III (Hambly et al. 2001b) is concerned with astrometry. These latter two papers contain much technical information about the SSS. This paper summarises that information and compares with similar data from other survey programmes. We also describe how to access the data and give examples of results from the SSS.

Astronomical photography, which revolutionised astronomy in the late nineteenth and early twentieth centuries, has a history almost as long as that of photography itself (Lankford 1984 and references therein). Digitised photographic sky surveys revolutionised astronomy in the late twentieth century; their evolution over the last few decades has been dictated by developments in microdensitometry and digital electronics (e.g. Klingsmith 1984; MacGillivray & Thomson 1992). Of course, in the modern era the sky is being digitised directly, bypassing photography altogether. This brings many advantages, not the least of which are the ability to survey faster, deeper and at wavelengths other than the optical – e.g. the Sloan Digital Sky Survey (SDSS, York et al. 2000) and the Two–Micron All–Sky Survey (2MASS, Kleinmann et al. 1994). However, it must be emphasised that for time–dependent phenomena for example (e.g. object position and brightness) photographic sky atlases represent a vast archive of invaluable measurements for *billions* of objects. This has been suitably demonstrated recently by the addition of Astrographic Catalogue measurements of the Carte du Ciel plates to Tycho positions from the Hipparcos mission (Urban, Corbin & Wycoff 1998; Høg et al. 2000 and references therein). This juxtaposition of

⋆ database available online at `http://www-wfau.roe.ac.uk/sss`

century–old photographic astrometry with a state–of–the–art space–based mission has yielded stellar proper motions on an unprecedented scale: *millions* of objects have proper motions measured to a precision of 2.5 mas yr^{-1}.

It was the development of the Schmidt telescope in the 1930s that revolutionised wide–angle photographic surveys (e.g. Cannon 1995). Along with developments in fast photographic emulsions, these enabled sky atlas production to faint limiting magnitudes. The 1.2m Palomar Oschin, 1.0m ESO and 1.2m UK Schmidt Telescopes have been systematically photographing the whole sky over the last half–century. Photographs have been taken in the blue, red and near–infrared passbands, with both blue and red passbands having observations at two epochs per field. For a concise summary of these photographic survey programmes, see Morgan (1995). Given the vast numbers ($> 10,000$) of plates in these sky atlases, it is clear that it is only through digitisation that these surveys can be fully exploited.

There are several major digitisation programmes completed or currently in progress. These projects consist of scanning various subsets of the available sky survey atlas photographs (in some cases glass or film copies of the original Schmidt photographs) and release of various data to the community. The scope of the various projects and their emphasis is different in each case. We now consider each in turn:

1.1 APM (Cambridge, UK)

The Automatic Plate Measuring (APM) machine is a 'flying–spot' microdensitometer with pixel size of 7.5μm (or 0.5 arcsec at the Schmidt plate scale of $\sim$ 67 arcsec mm^{-1}). For details concerning the APM hardware, see Kibblewhite et al. (1984); more information is also available at `http://www.ast.cam.ac.uk/~mike/casu/apm/apm.html`. The APM facility has produced the APM Northern Sky Catalogue (Irwin & McMahon 1992) which is based on scans of the first epoch Palomar (POSS–I) O and E glass copy atlases and covers the northern sky down to Galactic latitudes $|b| \geq 20^\circ$. This programme is currently being extended into the southern hemisphere using the SERC–J/EJ and SERC–ER/AAO–R surveys. The APM sky catalogues provide paired lists of blue and red objects with morphological parameters and image classification. Currently, they do not include pixel data, object proper motions or any information in the near–infrared. For more details, see the web pages accessed via the above URL.

1.2 APS (Minneapolis, USA)

The Automated Plate Scanner (APS) machine is described by Pennington et al. (1993) and is similar in design to the APM. This machine is also undertaking a scanning programme based on the POSS–I glass copies, but supplemented by the corresponding second epoch red plates obtained for the Luyten proper motion surveys (e.g. Luyten 1979 and references therein) and ultimately POSS–II. All 664 POSS–I fields having Galactic latitude $|b| > 20^\circ$ have been included. The APS object catalogue database (see `http://aps.umn.edu/`) is similar in content to that of the APM; proper motions will additionally be available in the future. Also, restricted numbers of plates have thresholded pixel data available online (the pixel size of the APS scans is 0.8 arcsec). These thresholded images have all sky areas set to zero intensity. Once again, no near–infrared data are available. For more information concerning the APS database, see Cornuelle et al. (1997).

1.3 COSMOS (Edinburgh, UK)

The COSMOS machine (e.g. MacGillivray & Stobie 1984), also a 'flying–spot' microdensitometer, was a development of the original GALAXY plate measuring machines (e.g. Murray & Nicholson 1975). COSMOS ceased operation in late 1993 and has now been superseded by SuperCOSMOS (see Section 1.6). The older machine had pixel size 1.1 arcsec and undertook a single colour (B_J) survey of the southern sky using the SERC–J/EJ atlas glass copies and UK Schmidt 'short' red (SR) originals at low Galactic latitude. The resulting database, the COSMOS/UKST Catalogue of the Southern Sky, included all fields at or south of the equator and having Galactic latitude $|b| > 10^\circ$ (J) or $|b| < 10^\circ$ (SR). For more details, see Yentis et al. (1992) and also Drinkwater, Barnes & Ellison (1995); an online database is available at `http://xip.nrl.navy.mil/`. The object catalogue contains position, morphological, photometric and classification information for each object in one colour (B_J or R depending on Galactic latitude). No pixel data, proper motions or near–infrared data are available.

1.4 DSS (Baltimore, USA)

Probably the greatest in scope of all the digitisation programmes is the Digitised Sky Survey at the Space Telescope Science Institute (Lasker 1992). This project was originally set up to provide guide stars for use with the Hubble Space Telescope (Jenker, Russell & Lasker 1988). Two modified PDS machines (known as Guide Star Automatic Measuring MAchines, or GAMMAs) were constructed for the purpose of scanning the photographic material, and the first generation scanning programme was implemented with 1.7 arcsec pixels. The surveys scanned consisted of the SERC–J/EJ, the POSS–I E and short exposure plates for fields having low Galactic latitude. The original Guide Star Catalogue (GSC–I, e.g. Lasker et al. 1990; Russell et al. 1990; Jenker et al. 1990) has since proven to be a major astronomical resource, far beyond its original goal of supporting HST operations. In addition, it was quickly realised that there was a large demand for the pixel data from the GSC–I scans, and the DSS has also become a major astronomical resource (for more information and online database access, see `http://archive.stsci.edu/dss/`). The volume of raw pixel data in the DSS–I necessitated the use of image compression techniques in order to make distribution possible (see Section 3.1.1). The second generation survey (DSS–II) is now nearly complete. This includes modified scanning hardware (the major change from DSS–I is that the pixel size is now 1 arcsec) and the addition of multiple colours and epochs from the POSS–II material in the northern hemisphere, and SERC–I/SERC–ER/AAO–R material in the south. A number of survey databases are in production. The second generation Guide Star Catalogue

(GSC–II) is under construction (McLean et al. 1997) and will include BRI colours as well as proper motion information, for all objects down to m $\sim$ 18. This catalogue is envisaged as being important for supporting various ground– and space–based instruments (e.g. Lasker et al. 1995). Compressed pixel data in the R band are being made available online at the above URL to supplement that available from DSS–I. Moreover, the Palomar–STScI Digital Sky Survey (DPOSS) is a project to archive and analyse the raw pixel data in each of the three colours (BRI) to the plate limits in every POSS–II survey field (e.g. Weir 1995 and references therein; Djorgovski et al. 1997). Once complete, the three–colour northern sky catalogue is expected to be released to the astronomical community.

1.5 PMM (Flagstaff, USA)

The Precision Measuring Machine (PMM) programme is operated at the United States Naval Observatory (USNO). The PMM uses CCD detectors to image (with 0.9 arcsec pixels) large regions of pairs of photographs simultaneously and very quickly; the machine and programme have been designed primarily with astrometric applications in mind. In addition to the CD–ROM stellar object catalogue products (containing paired lists of objects between blue and red plates with position and colour information only) – e.g. USNO–A1.0 (Canzian 1997), now superseded by USNO–A2.0 (Monet 1998) – the project now provides 'near–line' access to all the raw pixel data from the plate scans (see `http://www.nofs.navy.mil/data/FchPix/cfra.html`). Future products will include updated CD–ROM sets with object lists containing galaxies as well as stars, morphological information and proper motion data (e.g. USNO–B)

1.6 SuperCOSMOS (Edinburgh, UK)

The SuperCOSMOS machine is operated at Edinburgh and is the successor to COSMOS. SuperCOSMOS is a fast, high precision plate scanning facility with 0.67 arcsec pixels, 15–bit digitisation and accurate positional capability (e.g. see Miller et al. 1992 and Hambly et al. 1998). The origins of the survey programme (SSS) can be traced back several years (e.g. Hawkins 1992), and the SSS is the subject of this series of papers. Online database access and much additional information is available at `http://www-wfau.roe.ac.uk/sss`. In setting up the SSS programme, our intention has been to combine the best features of all of the above programmes to produce a versatile and easily used survey product with object parameter accuracy limited, as far as possible, by the source photographic material.

The above provides a very brief introduction to the enormous subject of digitised photographic sky surveys. For much more information, the reader is referred to conference proceedings by Capaccioli (1984), MacGillivray & Thomson (1992), MacGillivray et al. (1994), Chapman et al. (1995) and McLean et al. (1997a). For a general introduction to the subject of digitised sky surveys from Schmidt plates in particular, see Lasker (1995) and references therein.

2 DESCRIPTION

2.1 Summary of photographic material

For a complete description of the UK/ESO/Palomar Schmidt photographic atlases, see Morgan (1995) and references therein. In Table 1 we show the surveys which currently comprise the southern hemisphere SSS; in addition we show the corresponding northern hemisphere surveys that may be scanned. Note that, in some cases, glass or film copies have been scanned as opposed to glass originals; note also that some fields have a recent non–atlas plate or glass copy plate of the original atlas plate substituted where the original was unmeasurable (e.g. because of severe degradation due to 'microspots' – see Morgan 1995). All of the scanning programmes listed in Section 1 have made use of copy material for some areas/passbands. Although no rigorous quantitative assessment has been done, it is generally thought that the use of copy material is not significantly detrimental to the accuracy of the scanned data. The system of field numbers used by the UK and ESO Schmidt telescopes is described in Tritton (1983) and consists of uniformly–spaced field centres at a 5° pitch with $\sim 0.5^\circ$ overlap at all boundaries (for the UK Schmidt plates); this survey system was reflected into the northern hemisphere and adopted for the second epoch Palomar Sky Survey (POSS–II). The first epoch Palomar Sky Survey (POSS–I) used 6° field spacing on a different grid (see Minkowski & Abell 1963) resulting in little overlap between each field. A description of the scanning procedure used to digitise the photographic material is given in Paper II and references therein.

2.2 Database organisation and access

SSS data are available in the form of pixel images and/or object catalogues. Figure 1 gives a schematic illustration of the user interface, summarising the main features. The database organisation and modes of access are quite general, and allow specification of the colour of interest for image queries, and equivalently the 'master' colour (or colour of most interest) for object catalogue queries. Object catalogue information from other colours for the same objects/areas is given for both image and object catalogue queries. The concept of a user–specified master (or reference) colour allows an object catalogue query aimed at studying blue objects, for example, to specify the bluest plates in the collection as the data of most interest. In this way, objects not appearing on the redder plates will not be rejected if they are detected on the blue plates only. Presently, complete lists of objects appearing in all colours are not generated, although it will of course be possible to do this once the photography and scanning are complete. For a 'cookbook'–style introduction to access and browsing, the reader is referred to Hambly & Read (2000).

2.2.1 Image data

Each digitised Schmidt plate produces $\sim$ 2 Gbyte of 10 μm ($\sim$ 0.7 arcsec) pixel data (Paper II). A full–sky survey in three colours, one colour at two epochs results in $>$ 10 Tbyte of raw pixel data. In order to be able to store the pixel data *and* the associated multi–parameter object catalogues online for fast access, we have employed the H–compress algo-

Survey	Dec centres	Plate limit	Dates of observation	Reference
Southern hemisphere survey:				
SERC–J/EJ[1]	$\delta \leq 0°$	$B_J \sim 23$	1974 to 1994	Cannon (1984)
SERC–ER/AAO–R[2]	$\delta \leq 0°$	$R \sim 22$	1984 to 2000	Cannon (1984); Morgan et al. (1992)
SERC–I	$\delta \leq 0°$	$I \sim 19$	1978 $\longrightarrow$	Hartley & Dawe (1981)
ESO–R[3]	$\delta \leq -20°$	$R \sim 22$	1978 to 1990	West (1984)
POSS–I E[3]	$-18° \leq \delta \leq 0°$	$R \sim 20$	1949 to 1958	Minkowski & Abell (1963)
Putative northern hemisphere survey:				
POSS–II B[3]	$\delta \geq 0°$	$B_J \sim 22.5$	1987 to 1999	Reid et al. (1991)
POSS–II R[3]	$\delta \geq 0°$	$R \sim 20.8$	1987 to 1999	Reid et al. (1991)
POSS–II I[4]	$\delta \geq 0°$	$I \sim 19.5$	1989 $\longrightarrow$	Reid et al. (1991)
POSS–I E[3]	$\delta \geq 0°$	$R \sim 20$	1949 to 1958	Minkowski & Abell (1963)

Notes:
[1]Original glass survey plates scanned with the exception of the following 6 fields: 31, 102, 167, 330, 555, 575 (replacement glass originals).
[2]Original glass survey plates scanned with the exception of the following 32 field numbers: 52, 54, 111, 114, 119, 244, 296, 298, 355, 412, 413, 472, 473, 476, 483, 540, 541, 549, 550, 611, 619, 632, 679, 686, 691, 758, 760, 765, 828, 831, 837, 838 (film originals).
[3]Glass atlas copies of survey glass originals.
[4]Film atlas copies of survey glass originals.

Table 1. Photographic atlases comprising the SSS (after Morgan 1995); note that, at the time of writing, the I–band surveys are together incomplete at a total of ∼60 fields.

rithm developed at STScI (White et al. 1992) to compress the pixel data by a factor ~ 20. Note that SSS object catalogue data are derived from the *raw* pixel data before these are archived to tape for offline storage; however White et al. (1992) demonstrate the effect of image compression on astrometric and photometric performance. Furthermore, in Figure 3 (see Section 3.1 later) we show how image detection performs relative to uncompressed data as a function of compression factor to show quantitatively the effects of using H–compress. Clearly, there is no loss in 'depth' as measured by this test even for the relatively high compression factor of $\times 20$.

Pixel data extracted from the SSS database are currently provided in density units (Paper II, Equation 1) arbitrarily scaled to maximise use of the range of 16–bit integers per pixel. No photometric calibration is provided with the images since the dynamic range of the data are image–morphology dependent, and generally limited to around a factor ~ 2.1 in density (e.g. Hambly et al. 1998) which corresponds to a factor of ~ 10 in incident intensity; however approximate relative intensities for pixel values are given by $I \propto 10^{0.4D}$ where the exponent 0.4 takes into account the specularity of the SuperCOSMOS imaging optics.

Each image extracted from the database is output in standard Flexible Image Transport System format (see `http://heasarc.gsfc.nasa.gov/docs/heasarc/fits.html`) with comprehensive FITS header information giving details of the source photographic material, measurement and astrometric calibration. Additionally, FITS World Co-ordinate System keywords describing the local astrometry are included (see Paper III).

Each image extracted from the database also comes with an associated object catalogue so that the image data can be examined in conjunction with the detected sources in that area (e.g. by using GAIA/SkyCAT, Draper 1999). Two object lists are attached as binary table extensions to the image. The first table consists of the 'most useful' subset of all the image parameters available from the field/colour in question along with proper motion and colour information from other colours of the same field; the second table gives the remainder of the full 32 parameters set for each image from the plate of the specified colour. The equinox of the co-ordinates in object catalogues associated with images is always J2000.0 while the epoch is always that of the plate from which the positions are derived (as given in the FITS image header).

Presently, images up to 30 arcmin in size can be extracted online. Given an input position, the access software determines from which field the best image can be obtained (taking into account field overlaps and proximity to respective field centres).

2.2.2 Object catalogues

Image detection and parameterisation are described in Paper II. Each individual plate's pixel dataset has a raw object catalogue associated with it; each detected image has 32 parameters describing such quantities as position, brightness, morphology and image class. Photometric calibration is described in Paper II while astrometric calibration is described in Paper III. Object catalogue formats currently supported in the SSS are ASCII (i.e. plain text, the most human–readable format), the so–called tab–separated table (TST, Davenhall 2000 and references therein) and FITS binary table extensions. Paper II gives details of the internal storage units for object catalogue data (Table 1, Section 2.1.4). At

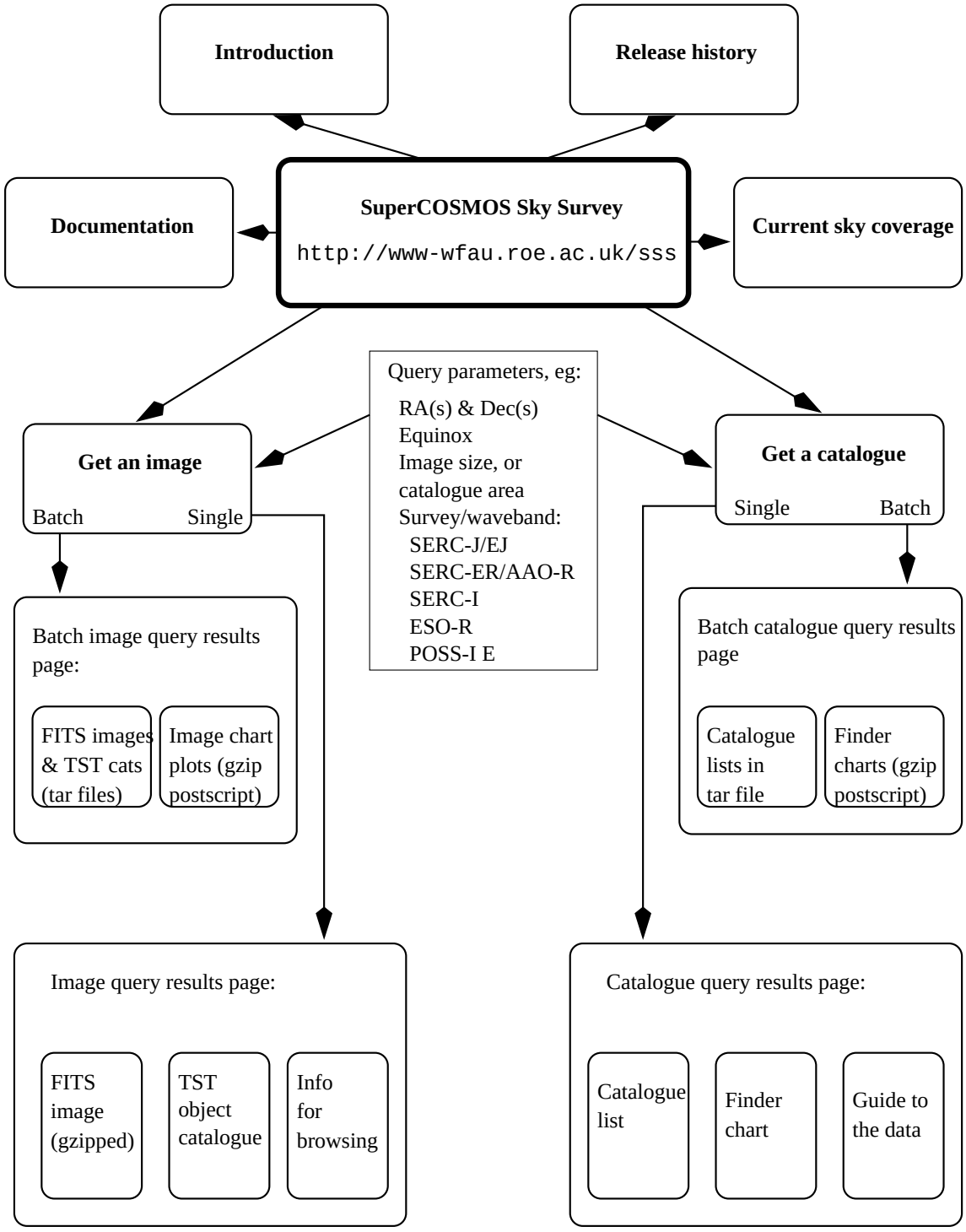

Figure 1. Schematic diagram illustrating the user interface to the SSS database.

access time, data are translated into more conventional units depending on which type of output file is being written. Note that for the TST and FITS formats, browsers and manipulation software may translate units internally for display purposes (for example, SSS FITS binary tables use double–precision floating point numbers in units of radians for celestial co-ordinates, and these will often be translated into sexagesimal for display).

ASCII format object catalogues (e.g. Figure 2) consist of object lists with sexagesimal celestial co-ordinates at the equinox/epoch specified by the user; proper motion measures and error estimates in units of mas yr^{-1} (defaulting to

RA (equinox J2000.0)	DEC	Epoch (J)	MU_ACOSD (mas/yr)	MU_D	SIGMU_A (mas/yr)	SIGMU_D	B(J)	R_1	R_2	I	Area (0.67" pix)	Ellipse (A, B, PA) (mas mas degs)	Class	N(0,1) (sigma)	Blend	Quality	Field No.
0 0 1.876	-00 9 48.54	1982.563	0.3121E+01	-0.6131E+01	0.1744E+02	0.1721E+02	19.857	99.999	18.463	17.813	58	2459 2061 168	2	2.420	0	0	823
0 0 9.988	-00 9 23.12	1982.563	0.9999E+09	0.9999E+09	0.9999E+09	0.9999E+09	22.803	99.999	99.999	99.999	8	1682 810 6	2	2.424	0	0	823
23 59 58.467	-00 9 19.43	1982.563	0.3692E+02	0.7453E+01	0.1775E+02	0.1751E+02	19.928	99.999	18.184	16.953	49	2133 1870 75	2	-0.984	0	0	823
23 59 45.689	-00 9 14.25	1982.563	0.9999E+09	0.9999E+09	0.9999E+09	0.9999E+09	22.330	99.999	99.999	99.999	12	1480 1049 146	2	-0.404	0	0	823
23 59 57.614	-00 9 13.28	1982.563	0.6081E+02	-0.4376E+02	0.3175E+02	0.3058E+02	21.841	99.999	20.381	99.999	20	2320 1171 108	2	1.757	0	0	823
0 0 13.049	-00 9 6.59	1982.563	0.1242E+02	-0.2594E+02	0.2853E+02	0.2755E+02	21.422	99.999	19.706	18.702	26	1796 1668 124	2	0.349	0	0	823
0 0 7.053	-00 9 4.35	1982.563	-0.1292E+03	0.8196E+01	0.3960E+02	0.3990E+02	21.150	99.999	20.356	99.999	39	3027 1479 103	1	3.626	0	0	823
23 59 51.113	-00 8 54.96	1982.563	0.1412E+02	0.2166E+02	0.3526E+02	0.3499E+02	20.752	99.999	19.293	99.999	50	3217 1891 112	1	6.059	0	0	823
23 59 49.019	-00 8 43.91	1982.563	0.3230E+02	0.7849E+01	0.3919E+02	0.3943E+02	21.112	99.999	20.197	99.999	42	2782 1991 130	1	5.125	0	0	823
23 59 41.500	-00 8 32.23	1982.563	-0.5762E+02	0.9149E+02	0.4976E+02	0.5140E+02	22.084	99.999	20.816	99.999	13	2126 1458 66	1	4.934	0	0	823
23 59 48.587	-00 8 22.20	1982.563	0.2966E+02	-0.1330E+01	0.4452E+02	0.4547E+02	21.602	99.999	20.373	99.999	28	2228 1707 151	1	2.773	0	0	823
0 0 17.351	-00 8 22.13	1982.563	0.9999E+09	0.9999E+09	0.9999E+09	0.9999E+09	20.329	99.999	99.999	99.999	33	2553 1423 75	2	-0.127	0	0	823
23 59 40.133	-00 8 21.48	1982.563	0.9999E+09	0.9999E+09	0.9999E+09	0.9999E+09	22.229	99.999	99.999	99.999	11	1562 1527 130	1	2.264	0	0	823
23 59 56.333	-00 8 16.47	1982.563	0.9999E+09	0.9999E+09	0.9999E+09	0.9999E+09	22.385	99.999	99.999	99.999	8	2990 590 48	1	3.907	0	0	823
23 59 55.329	-00 8 13.02	1982.563	0.7842E+01	-0.2252E+02	0.3572E+02	0.3550E+02	20.793	99.999	20.114	99.999	47	2528 2278 138	1	5.081	0	0	823
23 59 40.534	-00 8 12.55	1982.563	0.9999E+09	0.9999E+09	0.9999E+09	0.9999E+09	22.387	99.999	99.999	99.999	11	1300 1144 40	2	-0.574	0	0	823
23 59 51.482	-00 8 12.42	1982.563	0.2650E+02	-0.1061E+02	0.1360E+02	0.1231E+02	18.140	99.999	16.338	15.172	96	2749 2425 98	2	-0.256	0	16	823
23 59 58.223	-00 8 11.89	1982.563	0.3744E+02	-0.1400E+02	0.1458E+02	0.1251E+02	14.497	99.999	13.570	12.891	330	4850 4478 85	2	-1.195	0	16	823
0 0 6.223	-00 8 10.74	1982.563	0.9999E+09	0.9999E+09	0.9999E+09	0.9999E+09	21.743	99.999	99.999	99.999	18	2230 1441 24	1	5.052	0	0	823
23 59 52.295	-00 8 10.19	1982.563	0.9999E+09	0.9999E+09	0.9999E+09	0.9999E+09	22.120	99.999	99.999	99.999	18	1915 1388 52	1	2.331	0	0	823
23 59 51.239	-00 8 6.42	1982.563	0.9999E+09	0.9999E+09	0.9999E+09	0.9999E+09	22.097	99.999	99.999	99.999	15	1920 1200 161	2	-0.590	0	0	823
0 0 11.839	-00 8 5.05	1982.563	0.1311E+03	0.3713E+02	0.3739E+02	0.3589E+02	22.574	99.999	20.475	99.999	9	1315 853 6	2	-1.077	0	0	823
23 59 59.355	-00 8 3.09	1982.563	-0.6696E+02	-0.8103E+01	0.4263E+02	0.4332E+02	21.428	99.999	19.740	99.999	30	2477 2098 81	1	4.451	0	0	823
0 0 0.704	-00 8 0.21	1982.563	-0.5267E+01	-0.2974E+01	0.3995E+02	0.4030E+02	21.182	99.999	18.939	18.206	42	3599 1928 143	1	7.890	0	0	823
0 0 7.838	-00 7 54.90	1982.563	-0.6433E+01	-0.1794E+02	0.1458E+02	0.1251E+02	16.127	99.999	15.128	14.485	183	3599 3438 107	2	-0.677	0	16	823
0 0 11.822	-00 7 50.74	1982.563	0.9999E+09	0.9999E+09	0.9999E+09	0.9999E+09	22.790	99.999	99.999	99.999	8	1603 859 90	2	0.924	0	0	823
0 0 21.765	-00 7 45.19	1982.563	0.7109E+01	-0.4576E+01	0.1458E+02	0.1251E+02	15.877	99.999	15.170	14.775	202	3886 3461 98	2	0.092	0	16	823
23 59 55.012	-00 7 44.73	1982.563	0.9999E+09	0.9999E+09	0.9999E+09	0.9999E+09	21.962	99.999	99.999	99.999	17	2754 1283 168	1	3.693	0	0	823
0 0 16.483	-00 7 39.75	1982.563	-0.1723E+03	-0.4332E+02	0.3200E+02	0.3082E+02	21.873	99.999	19.821	99.999	20	1862 1599 160	2	0.933	0	0	823
0 0 21.222	-00 7 37.98	1982.563	0.3213E+01	0.4148E+01	0.1641E+02	0.1534E+02	19.509	99.999	17.907	17.122	54	2269 1824 110	2	-1.205	0	0	823
0 0 23.126	-00 7 34.66	1982.563	-0.1951E+02	0.4900E+02	0.3039E+02	0.2930E+02	21.664	99.999	19.680	18.315	19	1701 1474 47	2	-1.102	0	0	823
23 59 59.541	-00 7 33.42	1982.563	0.9999E+09	0.9999E+09	0.9999E+09	0.9999E+09	22.589	99.999	99.999	99.999	10	2685 663 112	1	2.093	0	0	823
0 0 3.547	-00 7 33.31	1982.563	0.9999E+09	0.9999E+09	0.9999E+09	0.9999E+09	21.991	99.999	99.999	99.999	16	1625 1207 78	2	-0.665	0	0	823
23 59 48.723	-00 7 32.80	1982.563	0.9999E+09	0.9999E+09	0.9999E+09	0.9999E+09	22.764	99.999	99.999	99.999	8	1646 771 117	2	0.617	0	0	823
23 59 59.613	-00 7 28.61	1982.563	0.9999E+09	0.9999E+09	0.9999E+09	0.9999E+09	22.559	99.999	99.999	99.999	8	1830 1157 82	1	2.225	0	0	823
23 59 34.002	-00 7 27.97	1982.563	0.9999E+09	0.9999E+09	0.9999E+09	0.9999E+09	22.704	99.999	99.999	99.999	8	2462 545 9	1	1.873	0	0	823
0 0 13.888	-00 7 27.65	1982.563	0.2021E+02	0.2952E+02	0.5887E+02	0.6171E+02	22.921	99.999	20.506	99.999	8	2184 487 7	1	-0.875	0	0	823
0 0 15.360	-00 7 26.62	1982.563	0.9999E+09	0.9999E+09	0.9999E+09	0.9999E+09	22.580	99.999	99.999	99.999	10	1783 1066 7	2	1.642	0	0	823
23 59 40.447	-00 7 24.03	1982.563	0.9999E+09	0.9999E+09	0.9999E+09	0.9999E+09	22.036	99.999	99.999	99.999	10	1013 933 0	4	-6.091	0	0	823
23 59 59.894	-00 7 18.30	1982.563	0.9999E+09	0.9999E+09	0.9999E+09	0.9999E+09	21.971	99.999	99.999	99.999	15	1577 1182 90	4	-2.668	0	0	823
23 59 58.762	-00 7 18.26	1982.563	0.1511E+03	-0.3571E+02	0.4561E+02	0.4670E+02	21.702	99.999	20.170	99.999	27	2945 1499 101	1	3.989	0	0	823
23 59 55.040	-00 7 17.70	1982.563	0.5928E+02	0.1165E+02	0.3177E+02	0.3060E+02	21.844	99.999	19.835	99.999	20	1895 1346 66	2	1.140	0	0	823
23 59 56.967	-00 7 12.87	1982.563	0.9999E+09	0.9999E+09	0.9999E+09	0.9999E+09	21.934	99.999	99.999	99.999	16	1642 1247 76	2	-0.689	0	0	823
23 59 33.815	-00 7 3.92	1982.563	0.2417E+02	-0.7612E+01	0.1600E+02	0.1434E+02	19.318	99.999	17.584	15.746	60	2322 2042 143	2	-0.296	0	0	823
0 0 18.784	-00 7 1.38	1982.563	0.9999E+09	0.9999E+09	0.9999E+09	0.9999E+09	21.785	99.999	99.999	99.999	22	2083 1809 74	2	1.860	0	0	823
0 0 1.293	-00 6 59.29	1982.563	-0.4529E+02	-0.6281E+02	0.1458E+02	0.1251E+02	14.445	99.999	13.170	12.577	372	4996 4696 78	2	0.825	0	16	823
23 59 55.243	-00 6 56.52	1982.563	0.9999E+09	0.9999E+09	0.9999E+09	0.9999E+09	22.074	99.999	99.999	99.999	16	2324 1291 10	1	3.391	0	0	823
23 59 48.969	-00 6 53.23	1982.563	0.9999E+09	0.9999E+09	0.9999E+09	0.9999E+09	21.294	99.999	99.999	99.999	31	2011 1911 3	2	1.973	0	0	823
23 59 34.579	-00 6 52.76	1982.563	0.1760E+02	-0.1396E+02	0.2256E+02	0.2193E+02	20.647	99.999	18.877	18.029	34	1882 1724 101	2	-1.026	0	0	823
0 0 25.304	-00 6 52.47	1982.563	-0.7569E+02	-0.4052E+02	0.3847E+02	0.3691E+02	22.714	99.999	20.126	99.999	8	1313 780 109	2	-0.505	0	0	823
23 59 39.781	-00 6 52.47	1982.563	0.1356E+02	-0.8476E+01	0.1377E+02	0.1251E+02	18.350	99.999	16.456	15.621	92	2630 2363 146	2	-0.362	0	0	823
23 59 55.722	-00 6 51.93	1982.563	0.2109E+01	0.9267E+01	0.3413E+02	0.3282E+02	22.150	99.999	20.585	99.999	12	1397 1131 85	2	-1.976	0	0	823
23 59 44.249	-00 6 49.54	1982.563	0.1502E+02	-0.2729E+02	0.1458E+02	0.1251E+02	12.612	99.999	11.974	11.505	757	7144 6894 132	2	-0.047	0	16	823
0 0 7.254	-00 6 48.42	1982.563	0.1751E+02	-0.1507E+01	0.1316E+02	0.1222E+02	17.861	99.999	16.869	16.375	101	2839 2514 130	2	-0.549	0	16	823
0 0 28.852	-00 6 45.04	1982.563	0.1139E+03	-0.6277E+01	0.3888E+02	0.3729E+02	22.767	99.999	20.669	99.999	8	1781 784 51	2	1.070	0	0	823
0 0 5.212	-00 6 43.51	1982.563	0.9999E+09	0.9999E+09	0.9999E+09	0.9999E+09	22.489	99.999	99.999	99.999	11	1903 823 43	2	1.728	0	0	823
0 0 18.273	-00 6 42.22	1982.563	-0.9069E+01	-0.1422E+02	0.1374E+02	0.1236E+02	18.228	99.999	17.187	16.580	92	2649 2526 176	2	-0.371	0	0	823
23 59 38.691	-00 6 41.39	1982.563	-0.1219E+02	0.6465E+02	0.2763E+02	0.2670E+02	21.306	99.999	20.139	99.999	30	2140 1734 169	2	1.599	0	0	823

Figure 2. Example object catalogue table from an SSS query.

9.99×10^8 if no measurement is available); BR_1R_2I magnitudes in the natural photographic systems (described, for example, in Bessell 1986 and Evans 1989 and references therein), defaulting to 99.999 when no measurement is available in any particular colour; morphological data from the master plate, including semi–major and semi–minor ellipse–fit axes in mas, celestial position angle in degrees, classification flag (1=non–stellar, 2=stellar, 3=unclassifiable and 4=noise) and profile classification statistic in units of sigma from an ideal stellar image (see Paper II, Section 2.2.3); image blending and quality information; and finally a field number of origin. TST files give the same information, but the units for the celestial co-ordinates are decimal degrees, as required by the TST standard. Furthermore, the ellipse–fit axes are given in units of 10 μm pixels, where 10 μm $\equiv$ 0.67 arcsec. FITS tables again give the same information, but celestial co-ordinates are stored in units of radians.

2.3 Object catalogue generation options

The online server giving access to the SSS data provides a number of options for object catalogue generation. These fall into the two broad categories of basic options, and those of a more advanced or expert nature.

Basic user options consist of: search centre and equinox; primary (or 'master') survey waveband, size of extracted area (rectangular or circular); primary magnitude range; output equinox; output epoch (celestial co-ordinates can be proper motion corrected to a given epoch, or alternatively left at the epoch of observation); and finally output format (ASCII, TST or FITS).

More advanced options (which default to sensible values for general queries) are: i) an option to purge or keep duplicate image in overlap regions; ii) subset of parameters or all 32 per object; iii) a blending option allowing one of four choices in the presence of blended images; and iv) an image quality threshold. The image analyser (described in Paper II) flags images according to detection of multiple components and various quality issues. The blend flag can be used to discard 'parent' images of multiple components (i.e. the single image comprising the components) or alternatively the component ('child') images may be discarded. The other two choices available are to keep *all* images (i.e. parents and children) or to keep only unblended images. If completeness is not an issue, then a clean catalogue of isolated, well defined images can be obtained using this last option. The quality bit flags are described in Paper II, Table 2 and a given quality threshold can be specified to discard images, since in general the more significant quality bits indicate more severe quality issues. For example, once again if completeness near bright stars is not an issue, a quality threshold of 1023 will reject all objects near a bright star as described in Paper II, Section 2.2.2. Since bit 10 in the quality flag is used to signify proximity to a bright star, and $2^{10} = 1024$, then any object having quality < 1024 is not affected by this particular quality issue – i.e. is not near a bright star. Conversely, a quality threshold of 2047 would *include* all those objects (and a good many spurious images due to diffraction spikes and low–level scattered light halos as well). The lower the quality threshold, the more strict the quality assurance is. Note that both blend and quality options are applied to every plate in creating the object catalogue (i.e. if other colours are available in addition to the primary colour, then the quality and blend tests are applied to their parameters also). All other selection options are applied to just the primary. Finally, the advanced options also include a pairing proximity choice of either 3 or 6 arcsec (the latter allows investigation of possible high proper motion objects – Paper III, Section 2.2.1) and a colour correction option allowing the switching on/off of correction of systematic errors as a function of position/magnitude (Paper II, Section 2.3.4).

2.4 'Seamless' catalogues and missing data

The modern Schmidt atlas surveys have varying degrees of overlap between adjacent fields. Also, the SSS is an on–going project requiring several years to complete the photography and scanning and, if data are to be made generally available as soon as possible, some data will be unavailable in specific areas. Moreover, paired information (i.e. colours and proper motions) are not always available if, for example, an image appears in one passband only. For all these reasons, a decision has to be made as to what to do in the case that more than one set of records, or no records at all, are available for given images or areas.

For the case of duplicate images in overlap regions the SSS database access software uses proximity to respective plate centres combined with quality information to decide which image to keep in the case that duplicates exist. Briefly, out of the list of duplicates available (which can be up to four in the extreme field corners), any having quality indicating proximity to a plate label or wedge (Paper II, Section 2.2.2) are discarded and then the object nearest the respective field centre is chosen as the 'best' image. Note that 'parent' images are unpaired in the database and will not be purged in overlap regions if selected.

For situations where paired information is not available (because the required data have not yet been included in the database, or because no image pairs with other colours exist) then null values are output for proper motions and colours. These are 9.999×10^8 for proper motion components and errors and 99.999 for magnitudes. Of course, in the case that no primary image records are available in a requested area, then nothing will appear in the extracted object catalogue dataset.

3 RESULTS AND DISCUSSION

3.1 Comparison with data from other scanning programmes

3.1.1 Pixels

For a quantitative comparison of the STScI and SuperCOSMOS pixel data products, a 30×30 arcmin region in ESO/SERC field 411 (i.e. at the South Galactic Pole) was chosen for test purposes. First (J) and second (R) generation DSS data were retreived from the STScI data server. These data are compressed by a factor ~ 10 to facilitate on–line storage at STScI; the SuperCOSMOS data were compressed using H–compress (White et al. 1992) by factors of 10 and 20 to compare directly with DSS data and also to show the effects of using higher compression factors. In

order to assess quantitatively and objectively the information content of the images, the data were run through PISA (Draper & Eaton 1999) which is an isophotal pixel analysis package similar to the COSMOS image analyser (Beard, MacGillivray & Thanisch 1990) that both ROE and STScI use to generate object catalogues (note of course that both groups provide object catalogues derived from uncompressed data; running decompressed images through object detection software is done here for illustrative purposes only). The data were thresholded (in density space) at 2.3σ above the mean sky level (Paper II, Section 2.1.4) and a minimum of 6 pixels was required to define an image in all cases. Note that this minimum pixel area cut was kept the same for the tests despite the fact that the STScI data have larger pixel sizes (25μm and 15μm for first and second generation data respectively), since reducing the cut for the coarser sampled data to an area equivalent to that of the higher resolution SuperCOSMOS data results in large numbers of spurious noise images being detected — it is fair to say that the fact that the SuperCOSMOS data has higher spatial resolution allows fainter detection limits, and this should be reflected in any test.

Figure 3 shows the results of the image detection tests when compared against a CCD image of the same field which reaches much fainter limits than the photographs. From the plots, it can be seen immediately that the SuperCOSMOS pixel data are superior (in this test, they reach ~ 1 mag deeper) than the DSS–I data, while the DSS–II and SuperCOSMOS data are broadly similar. Interestingly (and counter–intuitively), the image detection is deeper for higher compression factors. This has been noted before (e.g. White et al. 1992) and can be understood in terms of the compression algorithm smoothing the background which results in a lower detection threshold when computing $n\sigma$.

3.1.2 Astrometry

In Paper III, we demonstrate the external accuracy of the SSS data for $|b| \geq 30^\circ$ using the test described by Deutsch (1999) based on standard positions from the International Celestial Reference Frame (ICRF) sources listed in Ma et al. (1998). Table 2 summarises the results from Deutsch (1999) along with similar results from Paper III. In the Table, the columns $< \Delta\alpha >$, $< \Delta\delta >$ give the average offsets of the survey data from the ICRF sources; N is the number of sources used while $\Delta\alpha$, $\Delta\delta$ and ΔR are estimates of the scatter in the distributions in RA, Dec and radially (see Deutsch 1999 for more details).

Comparing figures in Table 2, the SSS data are as good as, or better than, all the other survey data. It should perhaps be emphasised that a mixture of reference catalogues have been used to astrometrically reduce the survey datasets used in Table 2 – e.g. Tycho–2 for APM and SSS data (Paper III); Tycho–AC for USNO–A2.0. Nonetheless, at the time of writing, these data were the best available.

Direct comparison of proper motion errors between the various surveys described in Section 1 was not possible at the time of writing due to the unavailability of the GSC–II and USNO–B catalogues. SSS proper motions are determined to be typically accurate to ~ 10 mas yr^{-1} in an absolute sense at m ~ 18 (e.g. Paper III). GSC–II proper motions are expected to be accurate to better than 4 mas yr^{-1} (McLean et al. 1997b); however it remains to be seen whether this is possible in the southern hemisphere, and whether it is a true absolute error (i.e. including any zeropoint errors) or merely a relative error under the most favourable conditions. As yet, there is no indication as to proper motion accuracy for USNO–B.

3.1.3 Photometry

Comparisons of catalogue photometry are even less clear than those for astrometric parameters. The absolute accuracy of photographic photometry will always be limited by position– and magnitude–dependent errors (Paper II); however as we have shown in the same paper, colours can be adjusted to remove such systematic errors from indices such as ($B_J - R$) or ($R - I$). Once again, it is as yet unclear whether such procedures will be used for many of the other surveys detailed in Section 1. In broad terms, GSC–II photometry is predicted to be accurate to 0.1–0.2 mag whereas GSC–I was only good to 0.4 mag (McLean et al. 1997b); an idea of the accuracy of colours for DPOSS may be obtained from Kennefick et al. (1995) – e.g. their Figures 1 compared with Paper II, Figure 10. SSS data are accurate in an *absolute* sense to $\sigma_{B,R,I} \sim 0.3$ (Paper II). However we note that SSS colours (e.g. $B_J - R$) are much more precise: $\sigma_{B-R} \sim 0.07$ mag at $B_J \sim 17$ rising to $\sigma_{B-R} \sim 0.16$ mag at $B_J \sim 20$. Colour indices are not susceptible to systematic errors (which dominate the single–passband precision of 0.3 mag) due to the calibration procedure described in Paper II, Section 2.3.4. The USNO catalogues are primarily for astrometric purposes, so a comparison of their photometric properties is inappropriate.

3.2 Science examples using SSS data

Applications of the SSS data are many and varied, ranging from the small–scale (e.g. finding–chart generation, secondary astrometric standards for deep images from other instruments/wavebands) through intermediate angular scales (e.g. statistical studies of the clustering properties of galaxies over degree scales) to the widest areas (e.g. statistical studies of the properties of galaxies averaged over large fractions of the whole sky).

Examples of small–scale applications of SSS data include optical identification of sources and registration of images from different wavebands (e.g. Galama et al. 1998; Jonker et al. 2000; Stairs et al. 2001). Degree–scale examples include identification of stellar samples from photometry (e.g. Preibisch & Zinnecker 1999) and the use of survey plate astrometry to provide a precise astrometric reference frame for fibre spectroscopy, for example open cluster work in IC 2391 (Barrado–y–Navascués et al. 2001) and NGC 2547 (Jeffries et al. 2000). In the remainder of this Section, we discuss some results from wide–angle studies employing SSS data.

3.2.1 Intrinsic alignments of galaxies at low redshift

The SGC subset of the SSS data has been used to attempt to detect the large scale structure of the universe via distortions in the shapes of background galaxies caused by gravita-

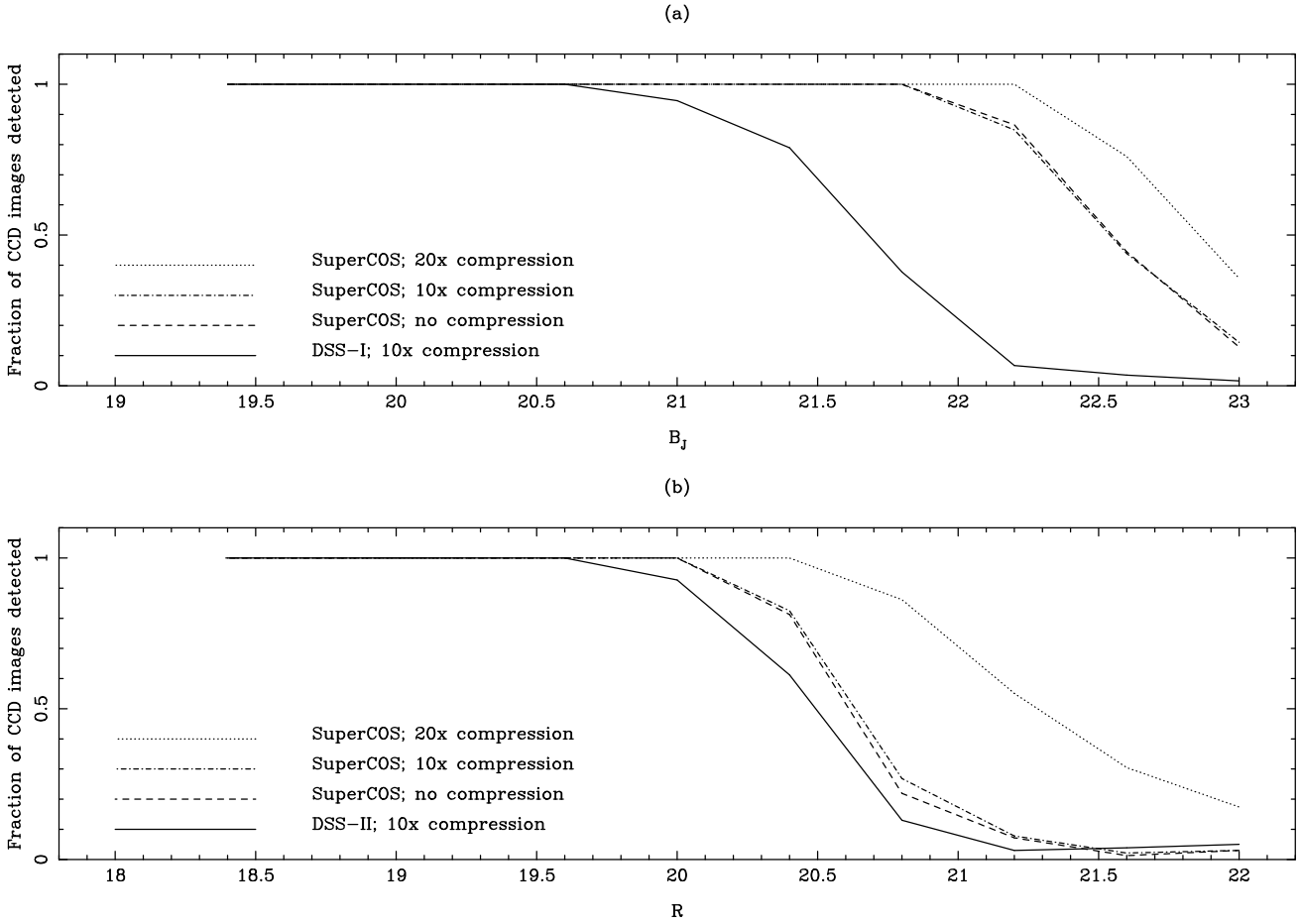

Figure 3. Number–magnitude histograms for (a) DSS–I, and (b) DSS–II with corresponding SuperCOSMOS data compared against deep CCD data in the SGP.

Database	$<\Delta\alpha>$	$<\Delta\delta>$	N	$\Delta\alpha$	$\Delta\delta$	ΔR	Note
	(arcseconds)			(arcseconds)			
SSS (J)	−0.05	−0.04	110	0.12	0.12	0.17	1
SSS (R)	−0.09	+0.07	103	0.14	0.23	0.27	1
USNO–A2.0	+0.04	+0.04	283	0.17	0.18	0.26	2
DSS–II(+1, −1)	−0.26	+0.07	235	0.63	0.52	0.85	3
DSS–I	−0.08	+0.03	274	0.53	0.48	0.75	
A2.0→DSS–I	+0.02	+0.03	104	0.18	0.19	0.32	4
A2.0→DSS–II	+0.04	+0.13	108	0.21	0.26	0.35	4
APM (UKST)	−0.06	+0.06	126	0.18	0.22	0.28	5
APM (POSS–I)	−0.05	+0.05	231	0.27	0.31	0.41	5

Notes:
1: SSS data from Paper III
2: USNO–A2.0 are the *average* of positions from J & R plates
3: results allowing for a 1 pixel offset in DSS–II image WCS (see Deutsch 1999)
4: results from using USNO–A2.0 to rereduce astrometry for DSS images
5: data from `http://www.ast.cam.ac.uk/~mike/apmcat`

Table 2. Empirical uncertainty estimates in survey astrometry relative to the ICRF (after Deutsch 1999; see also Paper III).

tional lensing by the intervening mass distribution. It turns out that the variance of galaxy ellipticities, σ_e^2 over some angular scale is a measure of this 'cosmic shear' effect over the same scale assuming that the background galaxies are initially randomly orientated (e.g. Kaiser 2000 and references therein). If this is not the case and there is some intrinsic preferential alignment of the background galaxies, then σ_e^2 will give an estimate of the size of this intrinsic alignment. Brown et al. (2001) have shown that, for a magnitude cut of $B_J < 20.5$ corresponding to a median galaxy redshift of

z ≈ 0.1, the galaxy ellipticities exhibit a non–zero correlation over scales between 1 and 100 arcmin. The variance of mean galaxy ellipticities is $\sim 10^{-2}$ at scales of ~ 10 arcmin and falls rapidly to $\sim 10^{-4}$ at scales of > 30 arcmin. Because of the low median redshift of the galaxies in the sample and the size of the signal it is concluded that the intrinsic alignment of galaxies has been measured, rather than the 'weak' lensing signal due to dark matter.

3.2.2 A survey for candidate Halo cool white dwarfs

Recently, there has been renewed interest in the possibility that a significant fraction of the Galactic Halo dark matter may be in the form of cool, ancient Halo white dwarfs (eg. Hodgkin et al. 2000; Ibata et al. 2000 and references therein). Wide–field, multi–epoch Schmidt data are ideal for searching for such objects, since they should have large intrinsic space motions and therefore large proper motions. The SGC subset of the SSS data have been analysed for high proper motion stars using the B and two R epochs to provide a clean, three–epoch sample with quantifiable completeness (see Hambly 2001 for more details). Follow–up spectroscopy on a large sample of objects subluminous in reduced proper motion has uncovered a significant number of new cool white dwarfs; a preliminary analysis indicates that the contribution to the 'standard' dark matter Halo from these objects is at least $\sim 2\%$ (Oppenheimer et al. 2001).

3.2.3 Galaxy two–point angular correlation

In principle a measurement of the two-point correlation function of galaxies $\xi(r)$ can provide useful constraints on the cosmological parameters which govern the evolution of the universe. Also an understanding of its evolution with redshift and morphological type (roughly colour selected sub–samples) can reveal the required ingredients for consistent models of galaxy formation (Peacock & Smith 2000, Benson et al. 2000). In the absence of any distance information, one can compute the two–point angular correlation function $\omega(\theta)$ of the sky–projected distribution of galaxies, which is defined as the excess probability above a Poissonian distribution for finding a galaxy in the angular areas $d\Omega_1$ and $d\Omega_2$ separated by an angular scale θ; explicitly $dP_{12} = \bar{n}^2[1 + w(\theta_{12})]\ d\Omega_1\ d\Omega_2$. Although a less sensitive statistic than $\xi(r)$, $\omega(\theta)$ does not suffer from redshift space distortions.

We have measured $\omega(\theta)$ for a sub–sample of the SSS; the sub–sample is enclosed within a circular region around the SGP covering roughly 3400 square degrees and contains over three million galaxies to a depth of $B_J = 21$. The correlation estmates were computed using the simple statistical estimators $\hat{\omega}(\theta)_1 = 1 + < DD > / < RR >$ and $\hat{\omega}(\theta)_2 = 1 + < DD > / < DR >$ where $< DD >$ represents the expected number of measured galaxy–galaxy pair counts, $< RR >$ the expected number of random–random pair counts and $< DR >$ the expected number of galaxy–random pair counts in the angular range $\theta \rightarrow \theta + d\theta$.

The resultant measurements of $\omega(\theta)$ for four magnitude slices of thickness 0.58 in the range $17.0 < B_J < 19.3$ have been computed assuming Poissonian errors. The amplitude of $\omega(\theta)$ increases with brightness as expected. Quantitavely, a simple linear least squares fit to the power-law slope on scales < 1 degree gives for bright to faint slices $\delta = 0.57$, 0.61, 0.56 and 0.59, with errors of order ± 0.02; where $\omega(\theta) \propto \theta^{-\delta}$. This absence of evolution in δ affirms the angular clustering meaurements from the APM survey (Maddox et al. 1990).

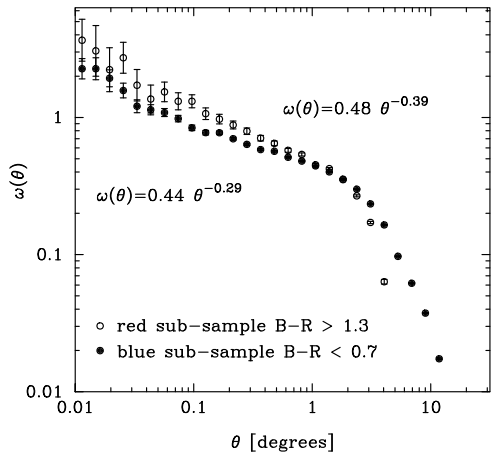

Figure 4. Galaxy two–point correlation function computed for red and blue galaxy samples within the SGC survey (see text).

In Figure 4 we compare the angular clustering for red and blue, colour selected sub–samples in the magnitude range $17.0 < B_J < 18.0$. We define blue galaxies to be those with $B_J - R < 0.7$ and red galaxies to be those with $B_J - R > 1.3$; the median $B_J - R$ for the survey is 1.1. We find that on scales $< 1^\circ$, red galaxies cluster more strongly than blue and that on scales $> 2^\circ$, blue galaxies are more strongly correlated (cf. Brown, Webster & Boyle 2000). Our interpretation of these two results is that red galaxies trace the clusters and since these are high peaks in the density field cluster more strongly on small scales; whereas blue galaxies have a higher propensity to be found in the field, so trace the large filamentary structures. Further details of this work will appear in Smith et al. (2001).

3.2.4 A survey for objects exhibiting extreme variability

The SSS survey contains R–band data at two epochs, enabling investigation of object variability. Figure 5 shows four examples of sources showing extreme variability obtained using strict selection criteria (e.g. in image shape and blending flag) from the SGC subset. The first three objects are presumably Galactic stellar variables ($\Delta m > 5$) and are possibly Miras or Novae; the final example is apparently an old supernova ($m_R \sim 14$; plate epoch 1983.8) associated with the edge–on Scr spiral ESO 148–20. Checks in the database archive SIMBAD yield no known catalogued objects at these positions, so these are apparently new discoveries; many more are almost certainly present in the SSS data.

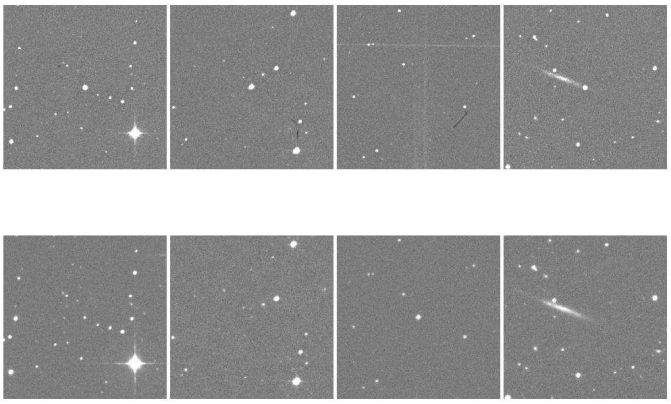

Figure 5. Four examples of objects showing extreme variability between the SSS R–band observation epochs (Δm > 5).

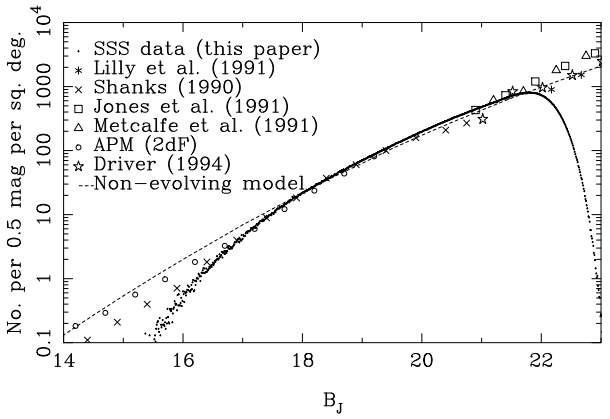

Figure 6. Number–magnitude counts for galaxies from the full SSS J data at Galactic latitudes $|b| > 45°$ along with comparison data from other surveys.

3.2.5 Number–magnitude counts for galaxies

In Figure 6 we show a recent compendium of galaxy counts spanning from the very local photographic surveys (e.g. SSS and APM) to deep CCD–based pencil–beam surveys. The SSS counts were made using all objects classed as galaxies and having $|b| > 45°$ in the full southern hemisphere survey. We extinction–corrected all galaxy magnitudes using $A_{\rm B_J} = 4.035 E_{\rm B-V}$ where $E_{\rm B-V}$ was derived from the maps of Schlegel, Finkbeiner & Davis (1998). A seamless catalogue was created with quality threshold set at 127 and deblended images were excluded (see Section 2.2). The SSS data agree very well with existing data. The dashed line shows the expected counts based on the most recent 2dF galaxy redshift luminosity function, the assumption of a flat zero–lambda cosmology and neglecting evolution. The model is normalised to the data at $\rm B_J = 19$. In general the model and data agree over the magnitude range $17.5 < \rm B_J < 21.5$. In detail the photographic data show some discrepancy from $\rm B_J \sim 20$ indicating the onset of selection bias. This is most likely due to increasing numbers of galaxies being unresolved on the plates (and therefore being classified as stars) and also the effect of surface–brightness dimming where some fraction of the distant population will be dimmed below the detection isophote. At the brightest magnitudes, the image detection algorithm 'breaks up' galaxy images leading to the underprediction with respect to the model and other surveys.

There are 1.65×10^7 galaxies in the catalogue used for this plot – the SSS data in Figure 6 are binned per 0.01 mag, normalised to 0.5 mag bin width. The smoothness of the curve demonstrates the extremely low sampling noise.

The web–based interface described in Section 2.2 allows object catalogue generation over areas up to ~ 100 square degrees. In this Section, we have described some science that is currently being done using local access to large area object catalogues comprising essentially *all* of the SSS catalogued data. It is envisaged that provision for web–based access to the whole database for such statistical analyses will be implemented in the medium term (see Section 5).

4 LIMITATIONS OF THE DATA

As is the case with any real imaging system, the procedure of automatic analysis of machine scans of photographs gives rise to various image and object catalogue artefacts that are spurious and yet may be mistaken for real phenomena in certain situations. Moreover, the pixel analysis and calibration procedures (Papers II and III) have their limitations; there are demonstrable systematic errors in some astrometric and photometric parameters in *all* data derived from photographic plates (e.g. the surveys described in Section 1). In this Section, we summarise some of these limitations and systematic errors in the SSS (some of which are described in more detail elsewhere in this series of papers) and in some cases describe techniques to minimise their impact when using the data.

4.1 Known systematic errors in photometry

As illustrated in Paper II, the absolute accuracy of the photometric calibration of any given passband are typically $\sigma \sim 0.3$ mag for m > 15. At the plate limit, this error is emulsion noise dominated and is essentially random (i.e. normally distributed). For magnitudes brighter than about 3 mag above the respective plate limits, the precision is limited by position– and magnitude–dependent systematic errors. For magnitudes brighter than m $\sim$ 14, systematic errors can become larger than ~ 0.5 mag depending on passband, field and position within the field. Note however that systematic errors in colours are eliminated using the technique described in Paper II, Section 2.3.4.

Note that the photometric calibration for stars and galaxies is different, and that the classification flag is used to decide which calibration and magnitude measure (isophotal or profile) are used when accessing the data. At the faint end where classification reliability is most likely to be poor the calibrations converge so systematic errors in photometry

from incorrect classification will be negligible. However, for bright images, incorrect classification (e.g. because of deblending errors) can produce incorrect magnitude calibration.

4.2 Known systematic errors in astrometry

In Paper III we show that the positional absolute astrometric accuracy is limited by field position dependent systematic errors for most images, resulting in errors with respect to the ICRF of typically ~ 0.2 arcsec with some dependence on passband and field position. A very small number of very low Galactic latitude B_J and R plates have absolute positional errors up to $\sim 3\times$ worse than this due to extreme crowding of the Tycho–2 astrometric standards. Such fields may be identified by examining the FITS headers for extracted images. Two keywords (`ASTSIGX` and `ASTSIGY`) are written with the WCS keywards which give the average residual of the Tycho–2 standards used in the global field astrometric solution (see Paper III); these figures may be taken as an indication of the likely level of any systematic errors within the field in such cases. Note that on scales of $\sim 0.5^\circ$ or less, and provided a field boundary is not being crossed, the systematic errors are constant so relative accuracy is typically better than 0.1 arcsec.

Proper motion errors are dominated by magnitude–dependent systematic errors for images brighter than m ~ 18 (Paper III). For a typical 15 yr baseline, the absolute accuracy of the proper motions is $\sigma \sim 10$ mas yr^{-1} in either co-ordinate.

4.3 Detection completeness and false detections at faint magnitudes

An indication of the detection completeness of SSS data is demonstrated in Paper II. With respect to deeper external data, SSS image catalogues are $> 90\%$ complete to within ~ 1.5 mag of the respective plate limits. For the SERC–J/EJ survey, this gives $> 90\%$ completeness to $B_J \sim 20.5$, and for the SERC–ER/AAO–R the same level of completeness to R ~ 19.5.

The question of noise detections at the plate limit is as yet unmeasured and is difficult to quantify theoretically. Although images are rigorously required to have 8 connected pixels with intensities $\geq 2.3\sigma$ above local sky (Paper II), the pixel–to–pixel noise is correlated to varying degrees in the image data. All that can be said here is that not every faint image will be real, and if clean and reliable datasets are required then it is advisable to use datasets paired between two or more colours when using SSS data. In any case, great care should be taken when using data within ~ 1 mag of the respective plate limits.

4.4 Limitations of deblending

Figure 7 shows an image and corresponding object catalogue ellipse plot from a 4×4 arcmin field at $(l, b) = (0.0^\circ, -15.0^\circ)$, demonstrating some limitations of the deblending algorithm (which are discussed in some detail in Beard et al. 1990). Briefly, deblending can only take place when rethresholding detects the fragmentation of an image; when a faint image is deblended from a bright image, object parameterisation (particularly the second moments) for the faint image can be badly affected. If completeness is not an important issue, then it is of course possible to use the deblending flag to choose only isolated images (e.g. Section 2.3). Figure 5 of Beard et al. (1990) demonstrates the relative completeness as a function of image density when deblending is/is not employed. At object densities of ~ 20 arcmin^{-2} (corresponding to $|b| \sim 10^\circ$ for example) completeness is $\sim 55\%$ without deblending whereas it is $\sim 75\%$ when deblended images are used.

For bright galaxy work, it is important to note that the image deblending algorithm tends to 'break up' such extended, structured images. In Figure 8 we show an example for the Cartwheel galaxy ($\alpha \sim 0^{\rm h}37^{\rm m}; \delta \sim -33^\circ43$). If bright resolved galaxies are of interest, then it may be advisable to ignore deblended images, and include only those images for which blend ≤ 0; however it should be noted that at present, parent images in the SSS database are unpaired, so colour information and 'seaming' in plate overlap regions are not available.

4.5 Image classification

Again, Paper II quantifies the reliability of image classification with respect to external datasets – a typical figure is $> 90\%$ reliability of correct classification to $B_J \sim 20.5$. However, it is important to note that two classification parameters are available for each image in each passband in SSS data: the discrete classification code or flag, and the normalised profile classification statistic η. The discrete code is defined as 4 (noise) for $\eta < -3.0$, stellar for $-3.0 \leq \eta \leq +2.0$ and non–stellar for $\eta > +2.0$. Hence, the classification flag is conservative in the sense of defining a clean but incomplete stellar sample. Some applications may require a less strict cut on image class (or a more strict cut on non–stellar class), in which case it may be advisable to use η as opposed to the flag to define, for example, a stellar selection having $-4.0 \leq \eta \leq +4.0$. This is equivalent to a k–sigma cut on the classification statistic, with corresponding confidence levels on stellar completeness assuming η is normally distributed for stars.

4.6 Image defects and spurious objects

Finally, we address the issue of image defects and spurious objects. As stated before, the combination of the photographic emulsion, digitisation and subsequent SuperCOSMOS pixel analysis is by no means a perfect imaging system. The following defects may be present in SSS data (more description of some of these may be found in Tritton 1983):

4.6.1 Emulsion microspots (very rare)

Figure 9 shows some examples of image data containing microspots, or emulsion flaws which appear over time on stored photographic material. These include classic 'gold spot', 'gold rings' and 'yellow spots'. Many of these flaws tend to be associated with higher density regions in the developed emulsion (e.g. around bright stars) and nearer the edges of the photographs. Where spotting was severe over

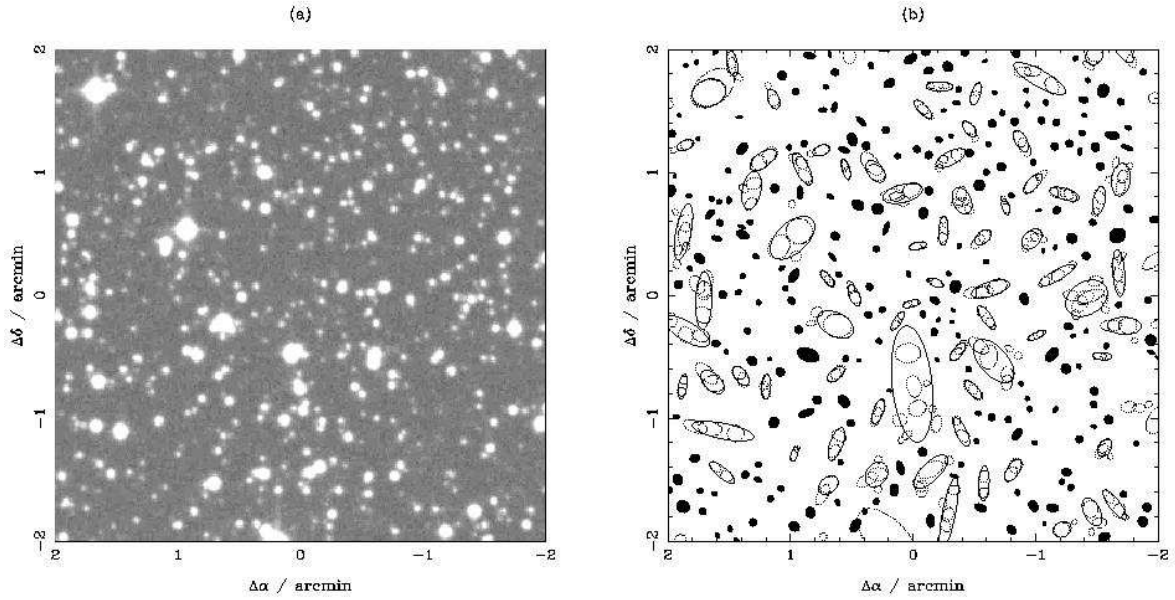

Figure 7. Illustration of the deblending algorithm at Galactic co-ordinates $(l, b) = (0.0°, -15.0°)$: (a) pixel data; (b) resulting image detections. Filled shapes are isolated images or images not detected as blends by the algorithm; solid line ellipses are parent images of blends while the deblended child images are shown as dotted ellipses. When faint images are blended with bright images, the image parameters can be adversely affected (see Beard et al. 1990).

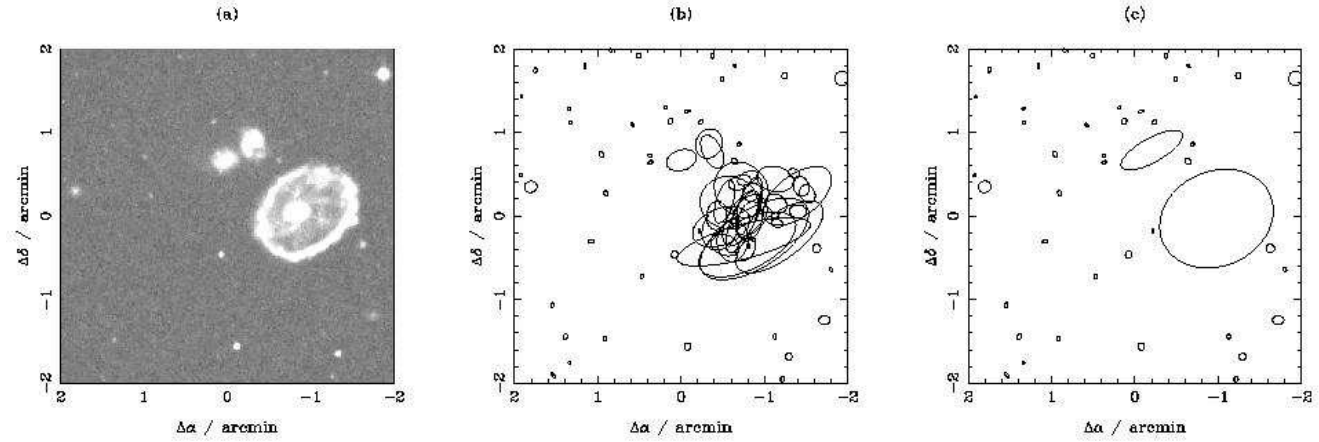

Figure 8. Example of image 'break–up' from deblending of the relatively bright Cartwheel galaxy: (a) J–band pixel data; (b) image detections employing deblended images; and (c) image detections with deblended images ignored.

large areas of the original atlas plates we have substituted a copy plate (made soon after the original was taken and developed) – see Table 1. Hence, the online digital data may differ from previously issued film atlases for example. Note that in the interests of a uniform survey we have limited substitution of originals by copies, and note also that where any spotting is present at the edges of fields, the adjacent plate overlap object data are generally available. Moreover, as shown in Figure 9, because microspots for the most part tend to produce higher transmission values than the sky level (i.e. apparent emulsion 'holes') they do not give rise to spurious object detections. However, one effect that has been noticed in the data is that bright images affected by 'gold rings' tend to be flagged as noise images by the image classifier, so in the very rare instances that microspots are present, image parameters may be affected.

4.6.2 Satellite trails (fairly common)

As an inevitable consequence of long exposures over wide angles in the modern age, many satellite trails are present on Schmidt atlas photographs. Moreover, trails resulting from meteors and other atmospheric phenomena can be present. Under pixel analysis, trails tend to fragment into a series of

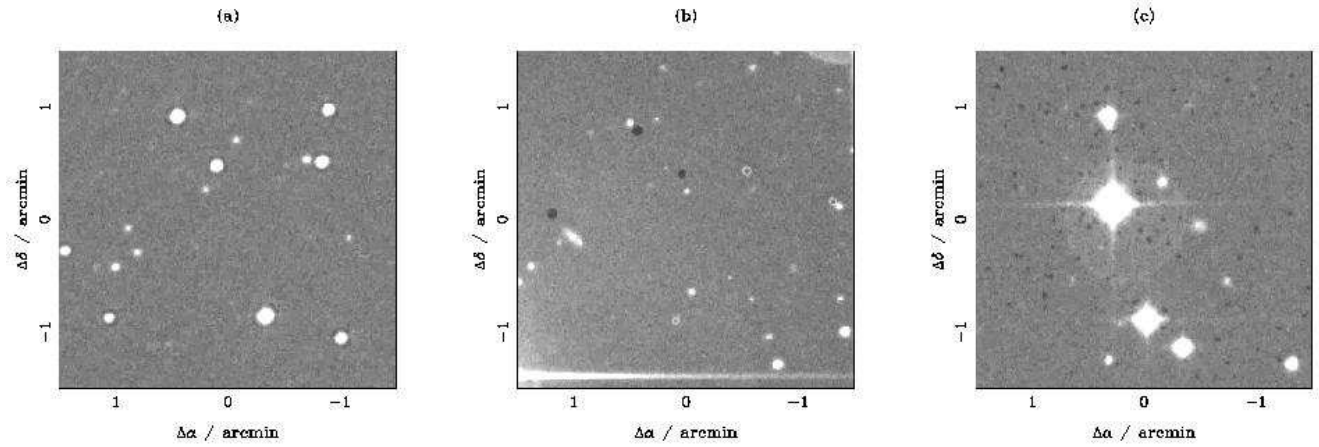

Figure 9. Some examples of emulsion microspots (artefacts darker than the sky in these images) in SSS imaging data (SERC–EJ): (a) 'gold rings' around brighter images; (b) 'yellow spots' near a bright image; and (c) an unusually severe case of 'yellow dots'.

faint, elliptical images classed as galaxies. The easiest way to eliminate such spurious detections from an SSS catalogue is to use a paired dataset – for example, Brown et al. (2001) used a B_J/R paired galaxy catalogue (i.e. a galaxy catalogue made by using the B_J plates as the master but in subsequent analysis only images with a corresponding R magnitude were used) despite the fact that the statistics were computed from the B_J data alone. For stellar work, an ellipticity cut can go a long way to eliminating spurious objects resulting from trails (as well as those from other sources – e.g. see the next Section).

4.6.3 Spurious images around bright stars (very common)

In Figure 10(a) and (b) we show B_J image data in the vicinity of a bright (m $\sim$ 10) star along with and ellipse plot of the raw image catalogue from those data. The remaining panels of Figure 10 show ellipse plots of object catalogues created by (c) performing an ellipse 'cut' of, somewhat arbitrarily, $e \leq 0.25$ (where $e = 1 - b/a$ and a, b are the semi–major and semi–minor ellipse axes); (d) by using the R–band magnitude to exclude stars that are unpaired between the B_J and R plates; (e) by switching off the deblending (i.e. including only those images with blend flag ≤ 0); and (f) by using the quality flag bit 10 to exclude all images within a circular area encompassing the spurious images (Paper II, Section 2.2.2). Clearly, there are advantages and disadvantages to each of these methods. For example, using the quality flag to 'drill' around bright stars is conservative in that *all* images (including real ones) are expunged from the circular region, while the ellipticity cut necessarily removes real galaxy images that are elliptical. The final method employed depends on the application, and must be left to the user, since there is a compromise to be made between contamination by spurious images and completeness of real objects.

5 CONCLUSION

We have presented a description of the SuperCOSMOS Sky Survey (SSS). We have described the properties of the SSS in relation to those of other digitisation programmes and presented examples of the use of the data. With reference to external data, we have illustrated the accuracy and reliability of SSS image parameters. Along with Papers II and III we have produced a comprehensive description and user guide for the SSS. Table 3 summarises the global properties of SSS object catalogue data.

At the time of writing, SSS sky coverage consists of full southern hemisphere (i.e. $\sim$ 20000 square degrees) in B_J and R; first–epoch R coverage is presently limited to the $\sim$ 5000 square degree SGC region while I band coverage is somewhat less than this. Projected dates for full completion of the southern hemisphere are $\sim$ mid 2002. At present, it is unclear whether the scanning programme will be extended into the northern hemisphere.

Apart from possible extension to whole–sky coverage, our future plans are as follows. Enhanced database access allowing fast, general queries to the entire dataset are being investigated; sophisticated database organisation (e.g. Szalay & Brunner 1997) and object–oriented design (Brunner 1997) are promising approaches. 'Release' of stand–alone, seamless object catalogues (e.g. for support operations at observatories) is desirable, and can be done when the survey is complete to some specified level. Other enhancements currently underway include addition of short exposure plates at low Galactic latitude (the UK Schmidt 'short red' survey, Hartley & Dawe 1981) for more reliable astrometry in crowded regions, and in future may include photometrically calibrated images, and proper motions based on the early epoch POSS–I 'E' plates for $\delta \geq -20°$. To a certain extent, enhancements and extensions depend on user demand from the community, and interested parties are encouraged to contact us directly if requiring large–scale exploitation of these data. The SSS homepage is `http://www-wfau.roe.ac.uk/sss`.

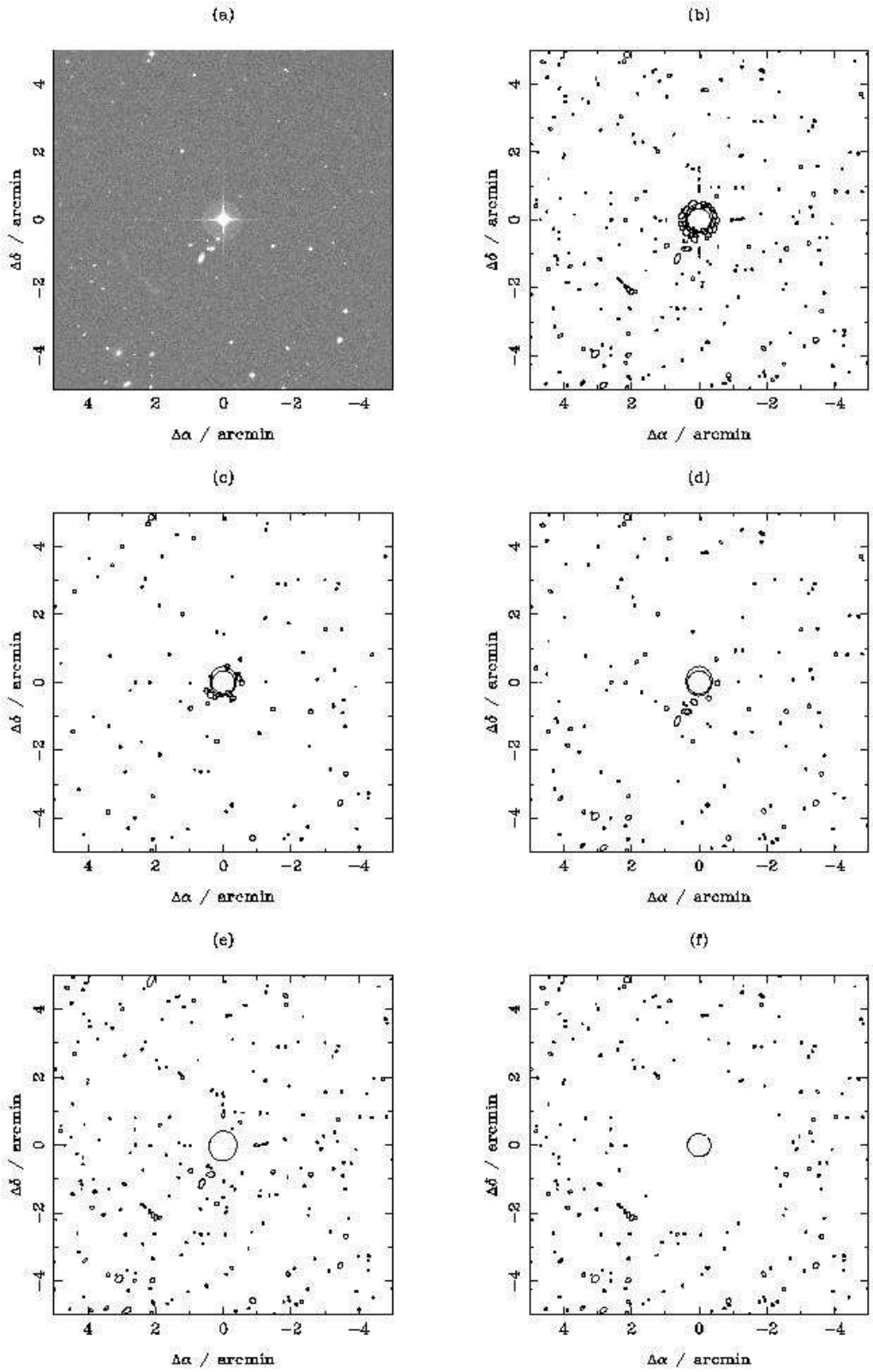

Figure 10. Spurious objects near a bright (m=10) star: (a) J–band pixel data; (b) all images detected; (c) images left after an ellipticity cut $e \leq 0.25$; (d) images having an R–band pair; (e) images left when deblending is not used; and (f) images left when using the quality flag to exclude all detections in the vicinity of the bright star. In (b), (c), (d) and (f) deblending is used (i.e. child images of blends are shown).

Astrometric properties:	Absolute accuracy	units
α, δ ($B_J < 19$)	0.1	arcsec
α, δ (faint images)	0.3	arcsec
proper motion $\mu_{\alpha,\delta}$ ($R < 17$)	10.0	mas yr^{-1}
$\mu_{\alpha,\delta}$ (faint images)	50.0	mas yr^{-1}
zeropoint error $\mu_{\alpha,\delta}$ ($R < 17$)	< 10.0	mas yr^{-1}
zeropoint error $\mu_{\alpha,\delta}$ ($R > 17$)	≤ 1.0	mas yr^{-1}

Photometric properties:	Accuracy absolute	relative	units
$\sigma_{B,R,I}$ ($< 19, 18, 17$)	0.3	0.05	mag
$\sigma_{B,R,I}$ (faint images)	0.3	0.3	mag
$\sigma_{(B-R)}$ ($B_J < 17$)	0.07	0.07	mag
$\sigma_{(B-R)}$ (faint images)	0.16	0.16	mag

Image detection/ completeness	external completeness	external reliability
$B_J < 19.5$	$\sim 100\%$	$\sim 100\%$
$B_J \sim 21$, $R \sim 19$	$\sim 75\%$	$\sim 90\%$

Table 3. Global properties of SSS object catalogue data (for these purposes, 'relative' means within restricted position and magnitude ranges). For more detailed information see Papers II and III.

ACKNOWLEDGEMENTS

The SuperCOSMOS Sky Survey project owes its existence and success to a large number of individuals. On the hardware side, many people at the former Royal Observatory at Edinburgh (now the United Kingdom Astronomy Technology Centre) were involved; particular thanks are due to Bill Cormack, Lance Miller, Magnus Paterson, Jim Herd, Janette Jameson, Tom Paul, Richard Bennett and Joel Sylvester. On the software side, we acknowledge the support of Steven Beard, Clive Davenhall, Bernard McNally and Mike Irwin. Obviously, the surveys would have been impossible without the diligence of many observers at the Schmidt telescopes, and many talented photographers in the development and copying laboratories. On the UK Schmidt side, we acknowledge the efforts of Malc Hartley, Ken Russell, Russell Cannon, Debi Allan, Fenella Stuart–Hamilton and Jason Cowan. Funding for the Wide Field Astronomy Unit at the Institute for Astronomy at the University of Edinburgh is provided by the UK PPARC. We acknowledge the use of STARLINK computing facilities at the Institute for Astronomy. We are indebted to the referee, Sean Urban, for a prompt and thorough review of these manuscripts.

The National Geographic Society–Palomar Observatory Sky Survey (POSS–I) was made by the California Institute of Technology with grants from the National Geographic Society. The UK Schmidt Telescope was operated by the Royal Observatory Edinburgh, with funding from the UK Science and Engineering Research Council (later the UK Particle Physics and Astronomy Research Council), until 1988 June, and thereafter by the Anglo–Australian Observatory. The blue plates of the southern sky atlas and its equatorial extension (together known as the SERC–J/EJ) as well as the Equatorial Red (ER), the second epoch (red) Survey (SES or AAO–R) and the infrared (SERC–I) Survey were taken with the UK Schmidt Telescope. All data retrieved from the URLs described herein are subject to the copyright given in this copyright summary. Copyright information specific to individual plates is provided in the downloaded FITS headers.

REFERENCES

Barrado–y–Navascués D., Stauffer J.R., Briceño C., Patten B., Hambly N.C., Adams J.D., 2001, ApJS, 134, 103

Beard S.M., MacGillivray H.T., Thanisch P.F., 1990, MNRAS, 247, 311

Benson A.J., Cole S., Frenk C.S., Baugh C.M., Lacey C.G., 2000, MNRAS, 311, 793

Bessell M.S., 1986, PASP, 98, 1303

Brown M.J.I., Webster R.L., Boyle B.J., 2000, MNRAS, 317, 782

Brown M.L., Taylor A.N., Hambly N.C., Dye S., 2000, MNRAS, submitted (astro–ph/0009499)

Brunner R.J., 1997, in McLean B.J., Golombek D.A., Hayes J.J.E., Payne H.E., eds, Proc. IAU Symp. 179, New Horizons from Multi–wavelength Sky Surveys. Kluwer, Dordrecht, p. 471

Cannon R.D., 1984, in Capaccioli M., ed., Proc. IAU Colloq. 78, Astronomy with Schmidt–type Telescopes. Kluwer, Dordrecht, p. 25

Cannon R.D., 1995, in Chapman J., Cannon R.D., Harrison S., Hidayat B., eds, ASP Conf. Ser. Vol. 84, The Future Utilisation of Schmidt Telescopes. Astron. Soc. Pac., San Francisco, p. 8

Canzian B., 1997, in McLean B.J., Golombek D.A., Hayes J.J.E., Payne H.E., eds, Proc. IAU Symp. 179, New Horizons from Multi–wavelength Sky Surveys. Kluwer, Dordrecht, p. 422

Capaccioli M. (ed.), 1984, Proc. IAU Colloq. 78, Astronomy with Schmidt–type Telescopes. Kluwer, Dordrecht

Chapman J., Cannon R.D., Harrison S., Hidayat B. (eds), 1995, ASP Conf. Ser. Vol. 84, The Future Utilisation of Schmidt Telescopes. Astron. Soc. Pac., San Francisco

Cornuelle C.S., Aldering G., Sourov A., Humphreys R.M., Larsen J.A., Cabanela J., 1997, in McLean B.J., Golombek D.A., Hayes J.J.E., Payne H.E., eds, Proc. IAU Symp. 179, New Horizons from Multi–wavelength Sky Surveys. Kluwer, Dordrecht, p. 467

Davenhall A.C., 2000, Starlink System Note No. 75.1: Writing Catalogue and Image Servers for GAIA and CURSA. CCLRC/Rutherford Appleton Laboratory, PPARC

Deutsch E.W., 1999, AJ, 118, 1882

Draper P.W., Eaton, N., 1999, Starlink User Note No. 109.10: PISA – Position, Intensity and Shape Analysis. CCLRC/Rutherford Appleton Laboratory, PPARC

Draper P.W., 1999, Starlink User Note No. 214.5: GAIA – Graphical Astronomy & Image Analysis Tool. CCLRC/Rutherford Appleton Laboratory, PPARC

Djorgovski S.G., de Carvalho R.R., Gal R.R., Pahre M.A., Scaramella R., Longo G., 1997, in McLean B.J., Golombek D.A., Hayes J.J.E., Payne H.E., eds, Proc. IAU Symp. 179, New Horizons from Multi–wavelength Sky Surveys. Kluwer, Dordrecht, p. 424

Drinkwater M.J., Barnes D.G., Ellison S.L., 1995, PASA, 12, 248

Driver S.P., 1994, PhD Thesis, Univ. Cardiff

Evans D.W., 1989, A&AS, 78, 249

Galama T.J. et al., 1998, Nature, 395, 670

Hambly N.C., Miller L., MacGillivray H.T., Herd J.T., Cormack W.A., 1998, MNRAS, 298, 897

Hambly N.C., Read M.A., 2000, Anglo–Australian Observatory Newsletter No. 92. Anglo–Australian Observatory, Sydney, p. 16

Hambly N.C., 2001, in Shipman H., Provencal J.L., eds, ASP Conf. Ser. Vol. 226, Proceedings of the 12th European Workshop on White Dwarfs. Astron. Soc. Pac., San Francisco, p. 381

Hambly N.C., Irwin M.J., MacGillivray H.T., 2001a, MNRAS, submitted (Paper II)

Hambly N.C., Davenhall A.C., Irwin M.J., MacGillivray H.T., 2001b, MNRAS, submitted (Paper III)

Hartley M., Dawe J.A., 1981, PASA, 4, 251

Hawkins M.R.S., 1992, in MacGillivray H.T., Thomson E.B., eds, Digitised Optical Sky Surveys. Kluwer, Dordrecht, p. 147

Hodgkin S.T., Oppenheimer B.R., Hambly N.C., Jameson R.F., Smartt S.J., Steele I.A., 2000, Nature, 403, 57

Høg E., Fabricius C., Makarov V.V., Urban S.E., Corbin T.E., Wycoff G.L., Bastian U., Schwekendiek P., Wicenec A., 2000, A&A, 355 L27

Ibata R., Irwin M.J., Bienaymé O., Scholz R., Guibert J., 2000, ApJ, 532, L41

Irwin M.J., McMahon R., 1992, in MacGillivray H.T., ed., IAU Working Group on Wide–Field Imaging, Newsletter No. 2, p. 31

Jeffries R.D., Totten E.J., Stauffer J.R., Barrado–y–Navascueés D., Hambly N.C., 2000, in Pallavicini R., Micela G., Sciortino S., eds, ASP Conf. Ser. Vol. 198, Proceedings of the conference on Stellar Clusters and Associations: Convection, Rotation and Dynamos. Astron. Soc. Pac., San Francisco, p. 281

Jenkner H., Russell J.L., Lasker B.M., 1988, in Barbat D., Eddy J.A., Eichhorn H.K., Upgren A.R., eds., IAU Symp. 133, Mapping the Sky. Kluwer, Dordecht, p. 239

Jenkner H., Lasker B.M., Sturch C.R., McLean B.J., Shara M.M., Russell J.L., 1990, AJ, 99, 2082

Jones L.R., Fong R., Shanks T., Ellis R.S., Peterson B.A., 1991, MNRAS, 249, 481

Jonker P.G., Fender R.P., Hambly N.C., van der Klis M., 2000, MNRAS, 315, L57

Kaiser N., 2000, ApJ, 537, 555

Kennefick J.D., de Carvalho R.R., Djorgovski S.G., Wilber M.M., Dickson E.S., Weit N., Fayyad U., Roden J., 1995, AJ, 110, 78

Kibblewhite E.J., Bridgeland M.T., Bunclark P., Irwin M.J., 1984, in Klingsmith, D.A., ed., Proceedings of the Astronomical Microdensitometry Conference. NASA Scientific and Technical Information Branch, Washington, p. 277

Kleinmann S.G., et al., 1994, Ap&SS, 217, 11

Klingsmith D.A. (ed.), 1984, Proceedings of the Astronomical Microdensitometry Conference. NASA Scientific and Technical Information Branch, Washington

Lankford J., 1984, in Gingerich O., ed., The General History of Astronomy, Part 4A: Astrophysics & Twentieth Century Astronomy to 1950. Cambridge Univ. Press, Cambridge, p. 16

Lasker B.M., Sturch C.R., McLean B.J., Russell J.L., Jenkner H., Shara M.M., 1990, AJ, 99, 2019

Lasker B.M., 1992, in MacGillivray H.T., Thomson E.B., eds, Digitised Optical Sky Surveys. Kluwer, Dordrecht, p. 87

Lasker B.M., McLean B.J., Jenkner H., Lattanzi M.G., Spagna A., 1995, in ESA SP–379, Future Possibilities for Astronomy in Space. ESA Scientific & Technical Publications Branch, Noordwijk, p. 137

Lasker B.M., 1995, PASP, 107, 763

Lilly S.J., Cowie L.L., Gardener J.P., 1991, ApJ, 369, L79

Luyten W.J., 1979, NLTT Catalog, Univ. Minnesota Press, Minneapolis

Ma C., Arias E.F., Eubanks T.M., Fey A.L., Gontier A.-M., Jacobs C.S., Sovers O.J., Archinal B.A., Charlot P., 1998, AJ, 116, 516

MacGillivray H.T., Stobie R.S., 1984, Vistas in Astronomy, 27, 433

MacGillivray H.T., Thomson E.B. (eds.), 1992, Digitised Optical Sky Surveys. Kluwer, Dordrecht

MacGillivray H.T., Thomson E.B., Lasker B.M., Reid I.N., Malin D.F., West R.M., Lorenz H. (eds.), 1994, IAU Symp. 161: Astronomy From Wide–Field Imaging, Kluwer, Dordrecht

Maddox S.J., Efstathiou G., Sutherland W.J., Loveday J., 1990, MNRAS, 242, 43P

McLean B.J., Golombek D.A., Hayes J.J.E., Payne H.E. (eds.), 1997a, Proc. IAU Symp. 179, New Horizons from Multi–Wavelength Sky Surveys. Kluwer, Dordrecht

McLean B.J., Hawkins G., Spagna A., Lattanzi M., Lasker B.M., Jenkner H., White R.I., 1997b, in McLean B.J., Golombek D.A., Hayes J.J.E., Payne H.E., eds, Proc. IAU Symp. 179, New Horizons from Multi–wavelength Sky Surveys. Kluwer, Dordrecht, p. 431

Metcalfe N., Shanks T., Fong R., Jones L.R., 1991, MNRAS, 249, 498

Miller L., Cormack W.A., Paterson M.G., Beard S.M., Lawrence L., 1992, in MacGillivray H.T., Thomson E.B., eds, Digitised Optical Sky Surveys. Kluwer, Dordrecht, p. 133

Minkowski R.L., Abell G.O., 1963, in Strand K.A., ed., Stars and Stellar Systems Vol. III: Basic Astronomical Data. Univ. Chicago Press, Chicago, p. 481

Monet D.G., 1998, BAAS, 30, 1427

Morgan D.H., Tritton S.B., Savage A., Hartley M., Cannon R.D., 1992, in MacGillivray H.T., Thomson E.B., eds, Digitised Optical Sky Surveys. Kluwer, Dordrecht, p. 11

Morgan D.H., 1995, in Chapman J., Cannon R.D., Harrison S., Hidayat B., eds, ASP Conf. Ser. Vol. 84, The Future Utilisation of Schmidt Telescopes. Astron. Soc. Pac., San Francisco, p. 137

Murray C.A., Nicholson W., 1975, in de Jager C., Nieuwenhuijzen H., eds, Image Processing Techniques in Astronomy. Reidel, Dordrecht, p. 171

Oppenheimer B.R., Hambly N.C., Digby A.P., Hodgkin S.T., 2001, Science, 292, 698

Peacock J.A., Smith R.E., 2000, MNRAS, 318, 1144

Pennington R.L., Humphreys R.M., Odewahn S.C., Zumach W., Thurmes P.M., 1993, PASP, 105, 521

Preibisch T., Zinnecker H., 1999, AJ, 117, 2381
Reid I.N., Brewer C., Brucato R.J., McKinley W.R., Maury A., Mendenhall D., Mould J.R., Mueller J., Neugebeuer G., Phinney J., Sargent W.L.W., Schombert J., Thicksten R., 1991, PASP, 103, 661
Russell J.L., Lasker B.M., McLean B.J., Sturch C.R., Jenkner H., 1990, AJ, 99, 2059
Schlegel D., Finkbeiner D., Davis M., 1998, ApJ, 500, 525
Shanks T., 1990, Bowyer S.C., Leinert C., Proc. IAU Symp. 139, Galactic and Extragalactic Background Radiation. Kluwer, Dordrecht, p. 269
Smith R.E. et al., 2001, in preparation
Stairs I.H. et al., 2001, MNRAS, 325, 979
Szalay A.S., Brunner R.J., 1997, in McLean B.J., Golombek D.A., Hayes J.J.E., Payne H.E., eds, Proc. IAU Symp. 179, New Horizons from Multi–wavelength Sky Surveys. Kluwer, Dordrecht, p. 455
Tritton S.B., 1983, United Kingdom Schmidt Telescope Handbook. ROE, Edinburgh
Urban S.E., Corbin T.E., Wycoff G.L., 1998, AJ, 115, 2161
Weir N., 1995, PhD Thesis, JPL/Caltech
West R.M., 1984, in Capaccioli M., ed., Proc. IAU Colloq. 78, Astronomy with Schmidt–type Telescopes. Kluwer, Dordrecht, p. 13
White R.L., Postman M., Lattanzi M.G., 1992, in MacGillivray H.T., Thomson E.B., eds, Digitised Optical Sky Surveys. Kluwer, Dordrecht, p. 167
Yentis D.G., Cruddace R.G., Gursky H., Stuart B.V., Wallin J.F., MacGillivray H.T., Collins C.A., 1992, in MacGillivray H.T., Thomson E.B., eds, Digitised Optical Sky Surveys. Kluwer, Dordrecht, p. 67
York D.G. et al., 2000, AJ, 120, 1579

This paper has been produced using the Royal Astronomical Society/Blackwell Science LaTeX style file.